THE JOURNAL OF PHYSICAL CHEMISTRY B

Article

pubs.acs.org/JPCB

Deciphering the Catalysis-Associated Conformational Changes of Human Adenylate Kinase 1 with Single-Molecule Spectroscopy

Chien Y. Lin,[†] Jung Y. Huang,*[,†,¶] and Leu-Wei Lo[‡]

[†]Department of Photonics, Chiao Tung University, Hsinchu, Taiwan

[‡]Division of Medical Engineering Research, National Health Research Institutes, Miaoli, Taiwan, R.O.C.

Supporting Information

ABSTRACT: Human adenylate kinase isoenzyme 1 (AK1) is the key enzyme in maintaining the cellular energy homeostasis. The catalysis-associated conformational changes of AK1 involve large-amplitude rearrangements. To decipher the conformational changes of AK1 at the single-molecule level, we tagged AK1 with two identical fluorophores, one near the substrate-binding site and the other at the boundary of the core domain. We found that magnesium ion binding to AK1 increases the structural heterogeneity of AK1, whereas ADP binding reduces the structural heterogeneity. We exploited the hidden Markov model to extract the underlying catalysis-associated conformational dynamics and determined thermodynamic parameters of the multiple catalytic pathways. The third-order correlation difference calculated from photon fluctuation traces reveals the irreversible nature of the conformational motions, suggesting that single-molecule AK1 is in a nonequilibrium steady state. This discovery offers a fresh viewpoint to look into the molecular mechanisms of cellular biochemistry.

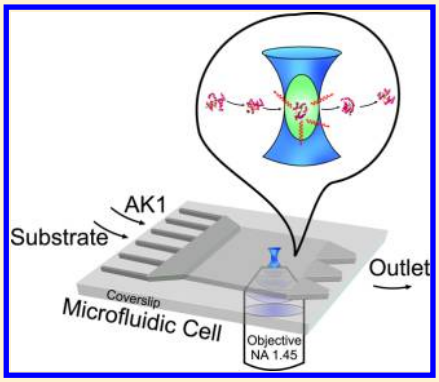

INTRODUCTION

Proteins are structurally flexible, spanning a wide range of motions from picoseconds to seconds.[1,2] Conformational changes in proteins are crucially relevant to a variety of biological functions.[3,4] For enzymatic proteins, mounting data suggest that large-scale protein motions play an important role in enzymatic turnover.[5−7] Many enzymes can also remodel themselves to optimize catalytic activity by adjusting the positions of critical amino acid residues and/or improving the thermal stability of the substrate-binding domain.[8,9] Quantitative description of the large-scale structural dynamics in the microsecond-to-second time scale is crucial for the understanding of the catalytic mechanism of an enzyme.

Adenylate kinase (AK) is the key enzyme in maintaining the cellular energy homeostasis by catalyzing the reaction of Mg^{2+}·ATP + AMP ⇌ Mg^{2+}·ADP + ADP in response to the cellular level of AMP.[10] AK comprises three relatively rigid domains, a central core (CORE), an AMP-binding domain (AMPbd), and a lid-shaped ATP-binding domain (ATPlid). During the catalytic cycle of AK, the largest conformational changes occur in the ATPlid and the AMPbd domains, while the CORE remains relatively unchanged. Figure 1 shows the conformation of AK in a ligand-free open form and ligand-bound closed form.

Conformational dynamics of AK from *E. coli* (AKE) has been investigated computationally with a variety of atomistic models.[11−13] Recent simulations on the free-energy landscape in the neighborhood of some conformational states show that ligand-free AKE can populate in multiple conformations. During the conformational dynamics, several metastable configurations exist to bridge the open and closed states of the enzyme.[11−13] Experimental revelation of the conformational dynamics of a protein by ensemble measurements is difficult because proteins do not move synchronously; therefore, the conformational dynamics is averaged away.[14,15] Observing a single molecule in action allows the hidden structural heterogeneity of a protein to be explored. Recently, a single-molecule fluorescence resonance energy transfer (smFRET) study has shown that ligand-free AKE populates in both the closed and open conformations in dynamic equilibrium. Interaction with the ligand shifts the conformational equilibrium toward the closed form.[3] NMR relaxation measurements suggested that the large-scale conformational changes associated with the ATPlid and AMPbd opening motion are the rate-limiting step of the catalytic turnover.[13] Despite this progress, the detailed catalysis-associated conformational dynamics such as ligand-binding, intermediate conformations along the minimum free-energy pathway, and cooperativity of individual domain motions remain elusive.

We employ a single-molecule fluorescent technique to decipher the catalysis-associated conformational changes of human AK isoenzyme 1 (AK1). The catalytic reaction of AK1 takes place in the core domain. It is crucial to know how the large-scale motions of two arms (ATPlid and AMPbd) distort the core domain after binding to the substrate. By using the self-quenching effect between two identical fluorophores, we are able to resolve the conformational changes of AK1 with

Received: February 25, 2013
Revised: October 16, 2013
Published: October 17, 2013

ACS Publications © 2013 American Chemical Society

dx.doi.org/10.1021/jp4019537 | J. Phys. Chem. B 2013, 117, 13947−13955

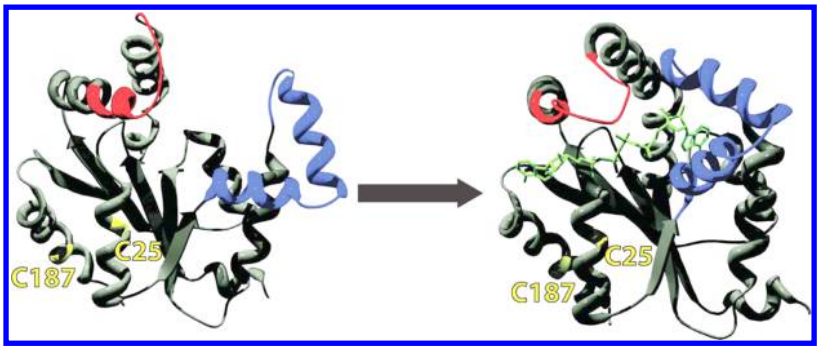

Figure 1. 3D models of AK1. (Left) Substrate-free AK1 in the open state is shown with different colors highlighting the CORE (dark gray), AMPbd (blue), and ATPlid (red) domains of AK1. C25 and C187 (the yellow-colored helical segments) indicate the positions of the two cysteine residues to be tagged with Alexa-532 fluorophores. The 3D structure of the substrate-bound AK1 (light green) in the closed state is shown on the right side. The 3D structures of substrate-free AK1 (3ADK) and substrate-bound AK1 (2C95) were taken from protein data bank, and the cartoon picture reproduced was by DeepView (http://spdbv.vital-it.ch).

high spatial resolution. We design a data-taking scheme to monitor the single-molecule dynamics for long time without the limitation of photobleaching. This strategy significantly improves the signal-to-noise ratio of our photon fluctuation measurements, which allows us to deduce the thermodynamic parameters of the enzyme's catalytic pathways.

METHOD

Sample Preparation and Enzymatic Activity Assay. Human AK1 (ab88049 from abcam) with a molecular weight of 21.6 kD has 194 amino acid residues. In the protein, the ATP-binding site covers the residues from 15 to 23, and the AMP-binding site is located at 94−101. To label AK1, an alkylation reaction of a maleimide with a sulfhydryl group of cysteine residue was employed. Maleimide reactions are very specific for sulfhydryl groups in the pH range of 6.5−7.5.[16] To prepare doubly tagged AK1, we used maleimide derivatives of Alexa Fluor 532 (from Invitrogen) to react with the two cysteine residues of AK1 (see Figure 1). One cysteine locates at C25 near the ATP-binding site, and the other (C187) locates at the boundary of the core domain. The reaction condition is 1.2 μM AK1 reacted with 12 μM chromophores in DMSO (pH = 7.0) at room temperature for 3 h. The 6 μM TCEP hydrochloride was added to prevent the formation of disulfide bonds in AK1. To ensure that the sample preparation yields doubly tagged AK1, we first used Sephadex G-25 Superfine column (GE Healthcare) to remove unreacted Alexa Fluor 532 from the solution. The solution was then brought to react with SulfoLink resin (Pierce) at room temperature for 30 min to remove AK1 species with unconjugated cysteine residues. From the measured optical absorption spectrum of the doubly tagged sample (see Figure S1 of the Supporting Information (SI)), we determine that 96% of AK1 molecules in the sample prepared are doubly tagged, which is better than that reported in the literature.[3]

C187, which is near the surface of AK1, has a higher probability to be immobilized at agarose-beads in a sulfhydryl-reactive affinity column (Thermo Scientific). We used this reactivity difference to prepare singly tagged AK1 species. We first allowed AK1 to react with a sulfhydryl-reactive affinity column at room temperature for 30 min. Each immobilized AK1 produces a pyridine-2-thione molecule, which absorbs strongly at 343 nm. We measured the absorbance to determine the molar concentration of the released pyridine-2-thione. With the measured value, we determined the coupling efficiency of the immobilized AK1 at C187 to be about 86%. The column was fluxed with a 10-time resin-bed volume of phosphate buffer to remove free AK1. We then added 5 mM TCEP in the column and waited for 30 min. The immobilized C187 of AK1 was released by reducing to thione, which cannot further react with maleimide derivatives. After collecting the solution, maleimide derivatives of Alexa Fluor 532 were added to react with the C25 residues of AK1 and form singly tagged species. The unreacted fluorophores in the reaction solution can be removed by G-25 Superfine column (GE Healthcare).

We conducted a catalytic activity assay on AK1 before and after fluorescent labeling by measuring the production rate of NADH. The peak absorbance of NADH at 340 nm increases linearly with reaction time (see Figure S2 of the SI). With an ADP concentration of [ADP] = 2 mM, 1 mg of native AK1, singly tagged AK1, and doubly tagged AK1 reveal a catalytic activity of 9.6, 9.0, and 10.1 U, respectively. By invoking the Michaelis−Menten kinetics, we can determine the Michaelis constant k_m and the maximum catalytic rate V_{max} from the measured optical absorption of NADH. We found that the catalytic activity differs by less than 11% between the native AK1 and doubly tagged AK1, indicating our labeling scheme to be an effective method to produce fluorophore-labeled AK1 with nearly intact catalytic activity.

Single-Molecule Fluorescent Measurement. For a smFRET study with two identical fluorophores, fluorescence anisotropy measurement is the only established method because in this case, the donors and acceptors are spectroscopically indistinguishable.[17] However, when van der Waals contact of the two identical fluorophores occurs, the fluorophore upon optical excitation can donate or accept an electron from the other fluorophore and return to the ground state without emission of a photon. This is called the photoinduced electron transfer (PET) effect.[18] At van der Waals contact, the two identical fluorophores can also form a dimer.[19,20] Recently, D. Setiawan et al.[21] investigated this effect with first-principles calculation. They discovered that the dimer molecular orbital of the lowest singlet excited state is always degenerate with one of the triplet excited states. Because this energy degeneracy is allowed by symmetry, we thought that the intersystem crossing in a dimer may be enhanced. To verify this conjecture, we employed a nonperturbative quantum evolution theory to derive the transition probability of the intersystem crossing, which is proportional to $(\varepsilon_S - \varepsilon_T + \varepsilon_{SO})^{-2}$. Here, ε_S, ε_T, and ε_{SO} denote the energy of the singlet state, triplet state, and spin−

orbit coupling, respectively. For a typical organic fluorophore, the energy difference ($\varepsilon_S - \varepsilon_T$) and spin−orbit coupling are about ∼1 and ∼0.01 eV, respectively. We estimate that upon forming a dimer with the energy degeneracy,[21] the transition probability of the intersystem crossing can be enhanced by a factor of $\sim 10^4$. The fluorescent efficiency of the dimer can be decreased because the optical excitation will be trapped in the triplet state, which has a long lifetime.[21] This self-quenching effect had been shown to be a sensitive probe for the conformational changes of a biomolecule with subnanometer resolution.[22]

The schematic diagram of our single-molecule optical measurement is shown in Figure 2a. AK1 molecules flow

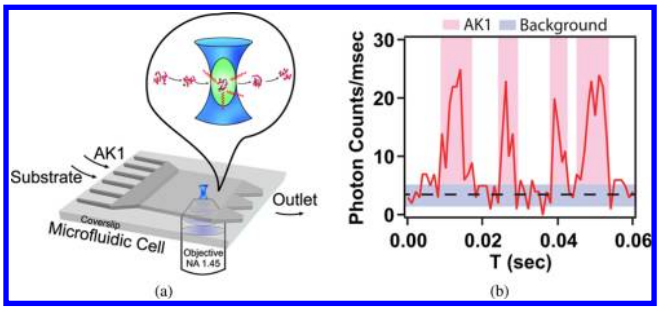

Figure 2. The experimental arrangement for single-molecule optical measurement. (a) A microfluidic cell controls the flow of AK1 molecules and substrates from two separate channels into a confocal region of a tightly focused laser beam. The fluorescent photon fluctuation signal containing the information of single-molecule conformational dynamics is detected with a single-photon avalanche diode. (b) A recorded short segment fluorescent signal trace. The optical background is marked by the dashed line with the standard deviation highlighted in light blue. The red solid line denotes the fluorescent signal from AK1, and the observation time windows for each AK1 molecules are emphasized with pink.

through the optical excitation region one by one. We estimated the traveling time of each molecules to be 6.8 ms with the flow speed of v_F = 28.1 μm/s and the excitation diameter $2\omega_0$ = 0.2 μm. The laser beam was circularly polarized to avoid any polarization-dependent signal variation. A 60 pM AK1 solution was prepared with a buffer containing 100 mM Tris-HCl (pH 7.5) and 100 mM KCl. The dilute solution and a pure buffer were flowed into a microfluidic cell (ONIX-262 Dynamic Cell Culture Platform fabricated by CellASIC, California) from two separate channels and mixed homogeneously in the optical excitation region. This concentration was chosen to let AK1 molecules flow through the optical excitation region individually with a separation time of 14 ms. A short segment of fluorescent signal emitted from AK1 is presented in Figure 2b. The effect of Mg^{2+} on AK1 can be studied by simply replacing the buffer with different Mg^{2+} concentrations. Similarly, we can flow a dilute AK1 solution and a buffer containing 2 mM Mg^{2+} and a variety of substrate (ADP) concentrations into the microfluidic cell to investigate the catalysis-associated conformational changes of AK1. For simplicity, hereafter, these AK1 species formed under a constant flow of ADP are called ADP-bound AK1.

Single-molecule fluorophores emit only a finite number of photons before being photobleached, which seriously limits the effective observation times. To circumvent this difficulty, we designed a data-taking scheme by utilizing the stochastic nature of single-molecule dynamics. Each AK1 molecule can be in any conformational state at the instant of entering into the optical excitation zone. In the phase space, each single-molecule trajectory traces out a region near the randomly selected state. After collecting a large number of short trajectories, each piece of information in the short single-molecule trajectories can be integrated to construct the complete conformational dynamics of AK1.

Data Analysis. For the data analysis, we first removed the background contribution from the photon fluctuation traces (see section 4 of the SI). The autocorrelation and the third-order correlation functions can then be calculated with the time-tag-to-correlation algorithm.[23] The resulting autocorrelation curves were fit to the diffusion and flow model[24]

$$g^{(2)}(\tau) = g^{(2)}(0)\left(1 + \frac{\tau}{\tau_D}\right)^{-1} \exp\left[-\left(\frac{\tau}{\tau_F}\right)^2\left(1 + \frac{\tau}{\tau_D}\right)^{-1}\right] \quad (1)$$

where $\tau_D = \omega_0^2/4D$ and $\tau_F = \omega_0/v_F$ are the diffusion time and the flow time of the AK1 molecule through an excitation beam waist ω_0. Here, D is the diffusion constant and v_F the flow velocity. We employed the two-time correlation difference, defined by $\Delta g^{(3)}(\tau_1,\tau_2) = g^{(3)}(\tau_1,\tau_2) - g^{(3)}(\tau_2,\tau_1)$, to fingerprint the nonequilibrium steady state (NESS), which is known to have a broken time permutation symmetry.

The hidden Markov model (HMM)[25,26] is useful to retrieve dynamic information from single-molecule data. According to the Bayes theory, the posterior probability distribution can be decomposed into a product of a prior and a likelihood distribution, normalized by the sum of marginal likelihood (i.e., the evidence). We use the marginal likelihood to score the goodness of fitting to a regression model. The model parameters include a number of hidden states and transition probabilities. To retrieve the model parameters, the HMM maximizes the marginal likelihood while penalizing overfitting with too many model parameters.[27] The marginal likelihood can be determined experimentally by projecting a fluorescent signal fluctuation trace (see, for example, Figure 2b) onto the y-axis and invoking a Gaussian mixture model to retrieve the central positions and the occurrences of the hidden states. The Gaussian mixture model is appropriate for the use because each hidden state has a unique conformation, which is perturbed by an environment with many degrees of freedom. That results in a system of hidden states well described by stochastically independent Gaussian processes. The HMM in a framework of variational Bayesian expectation maximization (VBEM)[28] was implemented in the Matlab code vbFRET, which is downloadable from the Website http://vbFRET.sourceforge.net.

For the HMM analysis, photon fluctuation traces were resampled with a 1 ms bin time. For each photon fluctuation trace, the HMM retrieval was executed by scanning the number of hidden states from 1 to 10. We calculated the corresponding evidence for each specific number of states. The maximum evidence yields the correct number of states. We labeled the photon fluctuation trace with the correct number of states using the Viterbi algorithm. For each photon fluctuation trace, we tested the HMM for 10 runs with different inputs. The HMM retrieval always returned the same number of states with a maximum evidence of $(1.01 \pm 0.01) \times 10^6$. In total, each states was retrieved from a photon fluctuation trace, containing ten million data points with 16 000 single-molecule events.

To test the applicability of the HMM for burst-like emission, we prepared a synthesized data set by assuming photons

dx.doi.org/10.1021/jp4019537 | J. Phys. Chem. B 2013, 117, 13947−13955

emitted from randomly selected states, which comprise the system background and three conformational states (closed, intermediate, and open states). The burst duration was fixed at 10 ms with a bin time of 1 ms. The HMM retrieval yields the correct number of states at the maximum evidence. The synthesized trajectory (red solid curve) and the corresponding HMM labeling output (blue dashed curve) are presented in Figure 3a. The agreement is excellent. Figure 3b shows the

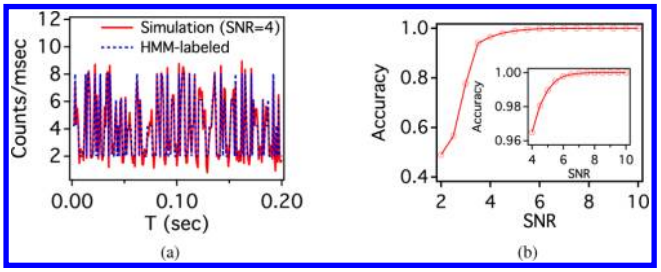

Figure 3. (a) A synthesized photon fluctuation trajectory with SNR = 4 (red solid curve) and the HMM-labeling output (blue dashed line). (b) The achieved accuracy of the HMM retrieval after accumulating one million data points of a fluorescent signal with different signal-to-noise ratios.

achieved HMM accuracy for one million data points with different signal-to-noise ratios. Our experimental measurements typically yield a signal-to-noise ratio of 4.5, indicating that the HMM labeling can achieve an accuracy of 98%.

RESULTS AND DISCUSSION

Verification of Single-Molecule Sensitivity. We present in Figure 4 the photon counting histogram (PCH) analysis[29] of

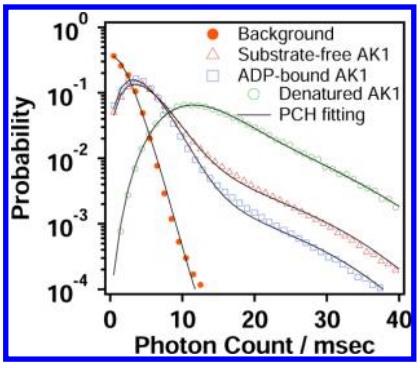

Figure 4. PCH curves of the system shot noise (solid circles) and photon signals emitted from doubly tagged AK1 in substrate-free (open triangles), ADP-bound (open squares), and denatured forms (open circles).

doubly tagged AK1 to verify that our photon fluctuation traces are generated from single-molecule species. From the PCH, we can determine the average number (N) of fluorophores in the optical excitation volume and the molecular brightness (E). In this figure, the system shot noise is shown by the red solid circles. The data from the substrate-free and the ADP-bound AK1 are presented with open triangles and open squares. For comparison, the data from an unfolded species formed by adding guanidine hydrochloride (Gdn-HCl) to denature the doubly tagged AK1 is shown by open circles. The substrate-free and ADP-bound AK1 exhibit a main peak at 3 counts/ms with a weaker shoulder at 30 counts/ms. The fitting results of PCH are summarized in Table 1.

Table 1. Results of PCH Analysis

PCH analysis	background	substrate-free AK1	ADP-bound AK1	denatured AK1
E1	2.2	2.9	2.6	3.1
N1	0.77	1.63	1.75	4.28
E2	29.1	31.4	31.2	27.1
N2	0.00	0.05	0.02	0.15

The fluorescent species flow unidirectionally in our single-molecule apparatus. The observation time is equal to the traveling time through a Gaussian beam region where the emitting signal is higher than the system noise level. Thus, fluorophores with lower brightness have a shorter observation time. The average number of photons emitted by the denatured AK1 is a factor of 2.3 larger than that from the substrate-free AK1. The effective observation time for the substrate-free AK1 is therefore 64% shorter than that for the denatured species. From Table1, by removing the system shot noise, the effective number of fluorophores in the substrate-free and ADP-bound AK1 was found to be 0.86 and 0.98, respectively. The effective number of fluorophores in the denatured AK1 can be estimated to be $4.28 \times 0.64 - 0.77 = 1.97$, indicating that the two fluorophores are far separated with a negligible self-quenching effect.

Self-Quenching Effect Encoding the Conformational Changes into Photon Fluctuation Traces. Three AK1 species were prepared to verify that the self-quenching probe is sensitive to reveal the conformational changes of AK1. The fluorescent signals from doubly tagged AK1 (red curve in the top panel), singly tagged AK1 (blue curve, middle panel), and denatured species (green curve, bottom pannel) are shown in Figure 5a. The corresponding PCH curves are presented in Figure 5b. Even though the doubly tagged AK1 possesses two fluorophores, the brightness per AK1 is weaker than that of singly tagged species, reflecting a strong self-quenching effect in the doubly tagged species. The denatured species produces the highest fluorescent intensity with a negligible self-quenching effect from the unfolded structure. This comparison strongly supports that our self-quenching probe can be used to monitor the conformational changes of AK1.

We can calculate the interburst time distribution from the photon fluctuation traces. The results are presented in Figure 5c. The distributions for the doubly tagged AK1 and the denatured species are almost identical, suggesting that each photon burst is generated by a single molecule, which agrees with the PCH analysis.

Mg^{2+}-Binding Increasing the Conformational Heterogeneity of AK1. Magnesium ion is an effecter in the cellular energy/signaling network.[30] The divalent ions can bind to negatively charged residues and reduce electrostatic interaction in a protein . We anticipate the secondary structure of AK1 to be perturbed by Mg^{2+}. Figure 6a shows the autocorrelation curves of fluorescent signals from doubly tagged AK1 in a buffer with different Mg^{2+} concentrations. We fit the autocorrelation curves to eq 1 to deduce $g^{(2)}(0)$, τ_D, and τ_F. The results are summarized in Table 2. Although both the pure diffusion model and the diffusion-flow model can be used to fit the autocorrelation functions, the diffusion-flow model yields smaller fitting residues. The AK1 concentration was chosen

dx.doi.org/10.1021/jp4019537 | J. Phys. Chem. B 2013, 117, 13947−13955

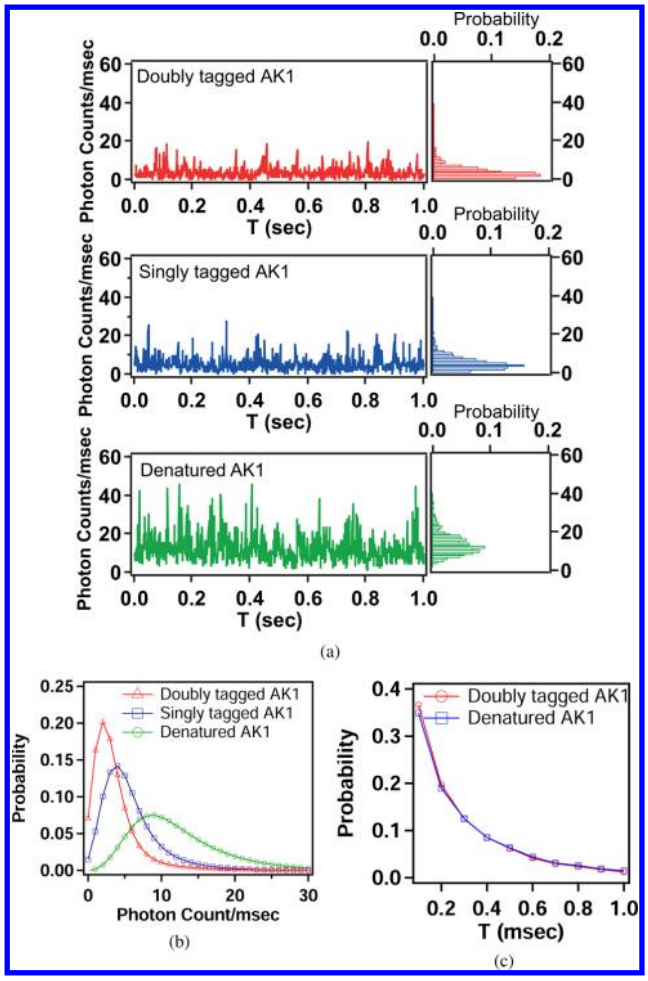

Figure 5. Fluorescent photon fluctuation traces emitted by different AK1 species. (a) Photon fluctuation signal from doubly tagged AK1 (red, top panel), singly tagged AK1 (blue, middle panel), and the denatured doubly tagged AK1 (green, bottom panel). (b) The corresponding histograms of the fluorescent emission rate from the three AK1 species. (c) The distribution of interphoton time deduced from the photon emission signal of doubly tagged AK1 in native and denatured forms.

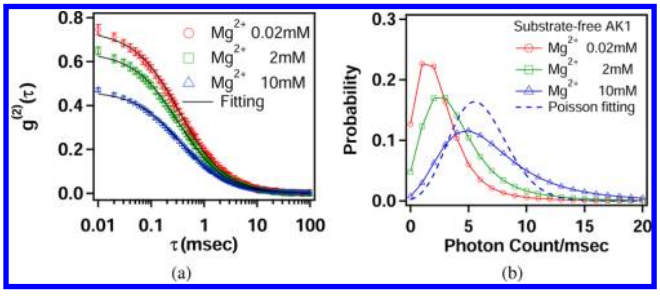

Figure 6. The influence of Mg^{2+} on AK1. (a) Autocorrelation functions (symbols) and the best fit to eq 1 (lines). (b) PCHs of fluorescent fluctuation signals from doubly tagged AK1 in a buffer with different Mg^{2+} concentrations (red circles: 0.02 mM; green squares: 2 mM; blue triangles: 10 mM). The Poisson distribution (dashed line) best fit to the PCH with 10 mM Mg^{2+} is included for comparison.

to allow AK1 molecules to flow through the optical excitation region one by one with a separation time of 14 ms. If AK1 molecules diffuse away from the optical excitation region without re-entry, the photon burst duration with a 1 ms bin time shall be limited by the diffusion time τ_D. We observed an exponential decaying histogram of burst duration with an average burst duration of 4.4 ms (see Figure S5 of the SI), which is longer than the diffusion time and reflects multiple re-entry events. With a 0.1 ms bin time, the histogram of burst duration shows an average burst duration of 0.2 ms, reflecting the diffusion process as reported in Table 2. Thus, in our single-molecule measurements, while the flow time τ_F = 6.8 ms determines the upper limit to the observation time of each molecule, the time in the beam is limited by diffusion-based residence or re-entry into the focal volume.

Table 2. Fitting Results of Autocorrelation Curves Shown in Figure 6a

$[Mg^{2+}]$	0.02 mM	2 mM	10 mM
$g^{(1)}(0)$	0.74	0.64	0.47
τ_D(ms)	0.35	0.33	0.35
τ_F(ms)	7.0	6.7	6.8

Because there are only a limited number of negatively charged residues in the ATPlid and the ATP-binding site of AK1, we anticipate that the effect of Mg^{2+} on fluorescent emission shall saturate when all negatively charged residues of AK1 have bound with Mg^{2+}. Instead, we found that $g^{(2)}(0)$ decreases from 0.74 for $[Mg^{2+}]$ = 0.02 mM to 0.64 for $[Mg^{2+}]$ = 2 mM and to 0.47 for $[Mg^{2+}]$ = 10 mM. The average fluorescence signal $\langle F \rangle$ also increases steadily (see Figure S4(a) of the SI) without any indication of saturation as the Mg^{2+} concentration is increased from 0.02 to 10 mM. Although we can straightforwardly attribute the increase to an increased quantum yield of Alexa-532, our measurement shows that Mg^{2+} slightly decreases the fluorescent quantum yield of Alexa-532. Thus, the observed fluorescence increase by Mg^{2+} for doubly tagged AK1 can only be attributed to a formation of less compact secondary structures of the protein.

The $g^{(2)}(0)$ is relevant to the variance of photon fluctuations.[31] Thus, the observed decreases of $g^{(2)}(0)$ by Mg^{2+} suggest that the conformational fluctuations of AK1 are suppressed by Mg^{2+}. The photon emission rate at time t reflects the conformational fluctuations observed in the time bin. The resulting PCH can be broadened by the conformational heterogeneity. We present the PCH of AK1 at different Mg^{2+} concentrations in Figure 6b and employ the Mandel's Q parameter,[32] defined as

$$Q = \frac{\langle F(t)^2 \rangle_t - \langle F(t) \rangle_t^2}{\langle F(t) \rangle_t} - 1 = S\langle E \rangle_t \qquad (2)$$

to quantify the conformational heterogeneity. Here, $F(t)$ is a fluorescent signal trace, $\langle \cdots \rangle_t$ denotes the time average, E is the molecular brightness, and S is the shape parameter relating to the point spread function (PSF) of the microscope used. The PSF-induced broadening can be estimated by measuring the PCH of free fluorophores, which shall have a Poisson distribution (Q = 0) due to vanishing structural heterogeneity. We found that the PCH of free Alexa-532 fluorophores deviates from a Poisson distribution by less than 1%, indicating the PSF-induced broadening to be negligible.

The Q parameter of AK1 in a buffer with 0.02, 2, and 10 mM Mg^{2+} was calculated to be 1.8, 2.1, and 2.4, respectively. We also present the Poisson distribution best fit to the PCH with 10 mM Mg^{2+} in Figure 6b to show the large deviation of the PCH from a Poisson distribution. It is interesting to know that the histogram of smFRET efficiency was recently found to be

dx.doi.org/10.1021/jp4019537 | J. Phys. Chem. B 2013, 117, 13947−13955

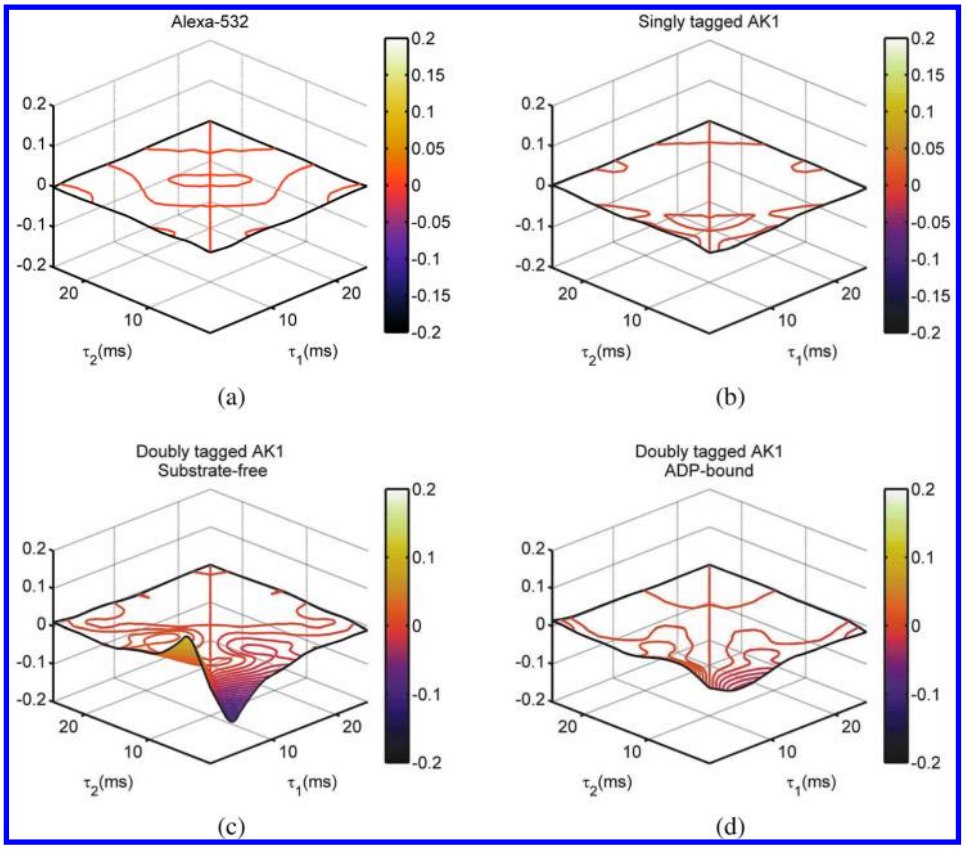

Figure 7. The difference of two-time correlation functions calculated using the fluorescent photon fluctuation traces from (a) Alexa-532 fluorophores free in a buffer, (b) singly tagged AK1, (c) doubly tagged AK1, and (d) ADP-bound doubly tagged AK1.

broaden by the conformational heterogeneity of a protein.[33,34] Molecular dynamics simulations had also revealed that a structural heterogeneity of 0.4−0.7 nm can exist in AKE due to a rugged free-energy landscape caused by the water molecules surrounding the ATPlid domain.[35] By summarizing these findings, we can attribute the decreasing $g^{(2)}(0)$ and increasing Q value with Mg^{2+} concentration to suppressed conformational fluctuations and higher conformational heterogeneity. Increasing the Mg^{2+} concentration may induce AK1 to pack in less compact forms that allow more water molecules to surround the ATPlid domain and yield a more rugged free-energy landscape.

All brightness measurements that employ a photon counting detector will be affected with the following two primary artifacts: Detector deadtime leads to a decrease in the number of photons and a narrowing PCH. Afterpulse will increase the number of photons detected, leading to a broadening of PCH. The nonideal detector effects modify the Q value as $\Delta Q = -2\tau_{dt}\langle F\rangle + 2p_{ap}$, where τ_{dt} is the deadtime and p_{ap} is the afterpulse probability. At our experimental photon counting rate (7 kcps), the τ_{dt}-induced uncertainty of Q is <3%. The uncertainty caused by the afterpulsing effect is <2.5% . The observed variations of Q at different experimental conditions are >10%. Therefore, the nonideal detector effects do not affect our conclusion with Q value measurements.

ADP Binding Reducing the Conformational Heterogeneity of AK1. Knowing how an AK1 catalyzes the phosphoryl transfer between ATP, ADP, and AMP on the single-molecule level is interesting. To answer this question, we first conducted an experimental study to investigate the structural changes of AK1 species. As shown in Figure 4, the PCH of doubly tagged AK1 is broader than that of ADP-bound species. The corresponding Q value for the substrate-free and the ADP-bound AK1 is 2.1 and 1.1, respectively, suggesting that ADP binding reduces the structural heterogeneity of AK1. The weaker photon fluctuation (revealed by a lower $g^{(2)}(0)$ of ADP-bound AK1; see Figure S3(c) of the SI) indicates suppressed conformational fluctuations by ADP binding. For comparison, the denatured species exhibits a Q value of 3.24, suggesting a much higher structural heterogeneity occurring in the unfolded structure than that in the native species.

Single-Molecule AK1 in a NESS. Molecular dynamics simulation[36] has shown that ligand-free AKE can dynamically sample multiple conformations along the minimum free-energy path, and the AMPbd closing follows the ATPlid in the ligand-free state. However, other molecular dynamics simulations on the nanosecond scale[37] predict an independent motion of ATPlid and AMPbd of AKE. Whether ordered motions in AK1 occur on the microsecond-to-second time scale remains unclear.

If ordered motions among different parts of AK1 exist, we anticipate to observe a high-order correlation in photon fluctuation traces. On the other hand, if the ATPlid and AMPbd domains move independently of each other, both the ATPlid-first-closing and the AMPbd-first-closing pathways are equally probable, and high-order correlation difference shall vanish. To test the conjecture, we measured the photon fluctuation traces of substrate-free and ADP-bound AK1. We calculated the second-order correlation function with

$$g^{(3)}(\tau_1, \tau_2) = \frac{\langle \delta F(t)\delta F(t+\tau_1)\delta F(t+\tau_1+\tau_2)\rangle_t}{\langle \delta F(t)\rangle_t^3} \quad (3)$$

dx.doi.org/10.1021/jp4019537 | J. Phys. Chem. B 2013, 117, 13947−13955

where $\delta F(t) = F(t) - \langle F(t)\rangle$. The resulting two-time correlation differences $\Delta g^{(3)}(\tau_1,\tau_2) = g^{(3)}(\tau_1,\tau_2) - g^{(3)}(\tau_2,\tau_1)$ are presented in Figure 7. For comparison, free Alexa-532 fluorophore and singly tagged AK1 were also included as references. As shown in Figure 7a and b, $\Delta g^{(3)}(\tau_1,\tau_2)$ for the free Alexa-532 fluorophore and singly tagged AK1 are essentially zero, indicating a high degree of time permutation symmetry in a single fluorophore, no matter whether it is free in solution or bound in a protein matrix. However, when the conformational changes of a ligand-free and ADP-bound AK1 are monitored correctly with self-quenching probes, the resulting $\Delta g^{(3)}(\tau_1,\tau_2)$ (see Figure 7c and d) are nonvanishing. For ADP-bound AK1, the main peak occurring at $\tau_1 \simeq 8$ ms is a factor of 3 weaker than that of substrate-free species. This is because upon substrate binding, the conformational dynamics of AK1 shifts toward the closed form, resulting in weaker conformational fluctuations. This high-order correlation result suggests that single-molecule AK1, which is driven by a constant flow of ADP or Mg^{2+}, is in a NESS. It is interesting to note that significant activity at $\tau_1 \simeq 8$ ms shown in Figure 7c occurs at the same time scale as the catalysis-associated conformational changes, suggesting that both the time irreversal NESS process and the catalysis-associated motions are regulated by the same mechanism.

A NESS system has to exchange energy with its environment and generate heat. According to the Clausius inequality $\Delta S \geqslant \int \delta Q/T\, dT$, an entropy shall also be produced.[38] Reactions in a NESS can be driven from sources to sinks between which a nonzero chemical potential difference must exist. If enzymes in a living cell are in a NESS, the biochemical networks catalyzed by these enzymes can then effectively adapt to the inhomogeneous cellular environment.

Two driving forces occur in our single-molecule AK1 experiment, which are the Mg^{2+} binding kinetics and the ADP-driven catalytic turnover. Why can Mg^{2+} ions drive AK1 into a NESS? To illustrate the mechanism, let us note that (i) AK1 is a protein with multiple conformations, (ii) Mg^{2+} can bind to AK1 at multiple sites, and (iii) the most distinguishing feature of a NESS is that energy must be supplied to maintain the NESS. If the association/dissociation processes of Mg^{2+} to AK1 are faster than the conformational changes of AK1, then after a few cycles, the reaction can occur in any conformational states of AK1. This shall cause the free-energy changes of the association/dissociation to depend on the conformational states of AK1. A net flux can then be generated to drive AK1 into a NESS. Our discovery of single-molecule AK1 in a NESS can be an important starting point to deepen our insight into the molecular mechanisms of cellular biochemistry.

Catalysis-Associated Conformational Switching in AK1. How can a NESS system generate a photon fluctuation trace with nonvanishing $\Delta g^{(3)}(\tau_1,\tau_2)$? To answer this question, HMM was employed to extract the catalysis-associated conformational changes of AK1.[28] Figure 8a shows one of the HMM labeling results for ligand-free AK1. Typically, six hidden states can be retrieved. We attribute the state with the lowest photon level to be the closed state. The intermediate state is metastable; therefore, the occurrence of this state shall be least sensitive to ADP addition. The remaining states are attributed to be partially open states and the fully open state. To facilitate further discussion, we used an occurrence-weighted average to represent the open and the partially open states. Thus, the photon fluctuation traces can be modeled to originate from transitions among the open (o),

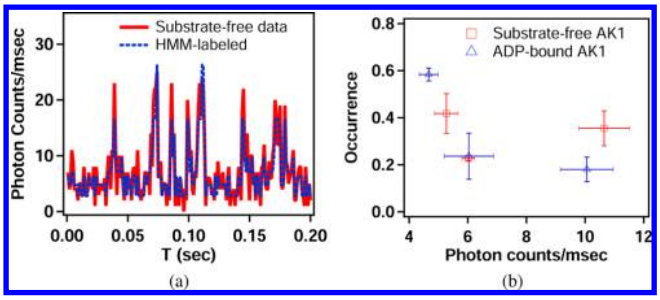

Figure 8. Results from HMM. (a) A photon counting trace (red solid curve) and the HMM-labeling result (blue dashed line). (b) The normalized occurrences of the conformation states (characterized by different photon counting rates) of substrate-free AK1 (red open squares) and ADP-bound AK1 (blue open triangles).

the intermediate (mid), and the closed states (c). Figure 8b shows the normalized occurrences of the three hidden states in ligand-free (open squares) and ADP-bound AK1 (open triangles). Compared to the ligand-free species, ADP binding shifts the conformational equilibrium toward the closed state, which is evidenced by higher occurrence of the closed state and lower occurrence of the open state. ADP binding also causes AK1 conformation in the open and closed states to be more compact, as revealed by lower photon emission levels.

Previous modeling and experimental studies have shown that AKE can assume a wide ensemble of conformations that differ by only a few k_BT. To probe into the conformational dynamics of AK1, the signal levels of each hidden state and the occurrences of transitions were retrieved. We fit the occurrence of the $a \rightarrow b$ transition to $N \exp[(-(x-a)^2 + (y-b)^2)/2\sigma_a^2]$ and determined the number of transition N and the variance σ_a^2, which is relevant to the conformational fluctuation of state a. The numbers of transitions are shown in Figure 9a for ligand-

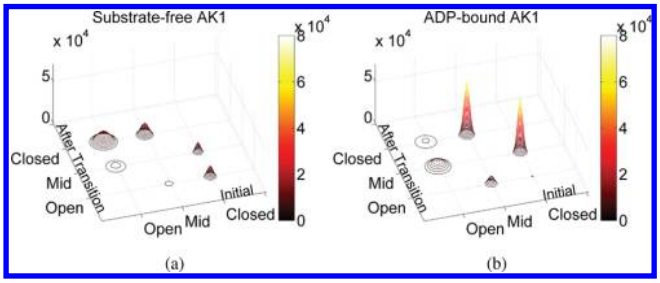

Figure 9. The occurrences of transitions in (a) substrate-free AK1 and (b) ADP-bound AK1 deduced from photon fluctuation traces with HMM.

free AK1 and Figure 9b for ADP-bound AK1. Significant increases in the mid ⇌ closed transitions were observed, which indicates that ADP binding promotes the mid-mediated pathway by suppressing the direct open-to-closed transitions.

The van't Hoff equation, which links kinetics (i.e., the reaction constant) and thermodynamics (the change in Gibbs free energy), can be used to yield $\Delta G_{ab} = -k_BT \cdot \ln(t_{w,b}/t_{w,a})$. The waiting time t_w at state a and b can be deduced from the numbers of transitions. By using the equation and relevant waiting times, we can determine the free-energy changes. The result for the mid-mediated pathway is shown in Figure 10b. We found that ADP binding can increase the free energy of the mid state by $0.34k_BT$, while it decreases the free energy of the closed state by $0.45k_BT$. This leads to an increase of

dx.doi.org/10.1021/jp4019537 | J. Phys. Chem. B 2013, 117, 13947−13955

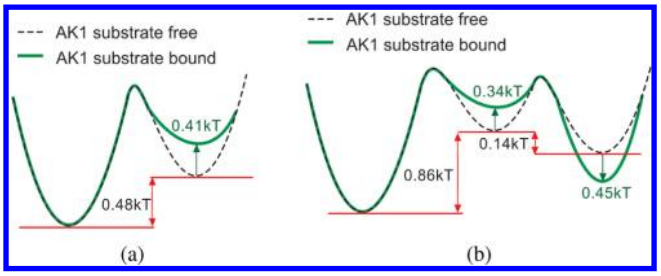

Figure 10. The catalytic pathways of AK1. (a) The direct open ⇌ closed (from left to right) pathway and (b) the mid-mediated open ⇌ mid ⇌ closed (from left to right) pathway.

$\Delta G_{mid\leftrightarrow closed}$ from $0.14k_BT$ to $0.93k_BT$. Recent theoretical study of the free energy of a long-chain polymer had shown that the free energy can be increased by a strain.[39] Inspired by the result, we attribute the free-energy increase in the mid state to be from a strain accumulated at the hinge region between ATPlid and CORE. The strain is released in the closed state by local unfolding and refolding of the α-helices in the ATPlid domain.[8] ADP binding also increases the free-energy change from $0.86k_BT$ to $1.2k_BT$ along the open-to-mid transition. However, after crossing the barrier, ADP binding can produce a larger free-energy decrease along the mid → closed process, resulting in a total free-energy cost of $0.27k_BT$ from the open to closed states. In contrast, the direct open ↔ closed pathway (see Figure 10a) has a higher free-energy cost of $0.89k_BT$ upon ADP binding. Therefore, although ligand-free species may prefer the direct open ↔ closed pathway, upon ADP binding, AK1 will switch to the mid-mediated pathway to gain the prize of the lowest free-energy cost.

The intermediate state plays a pivotal role in the catalysis of AK1. For the mid → closed process, the waiting time is 3.1 ms. It is reduced to 1.2 ms upon ADP binding. Longer waiting time implies a higher energy barrier to be surpassed in order to leave the state. Thus, ADP binding shall reduce the energy barrier height between the mid → closed state. The number of mid → closed transitions occupies about 46% of the total transitions in a substrate-free AK1. Upon ADP binding, the number of mid → closed transitions increases to 86%. The rate-limiting step in a catalytic turnover relates to the catalytic step that has the maximum free-energy change. From Figure 10b, the rate-limiting step of AK1 catalysis shall be the mid → open process (i.e., the opening of the ATPlid domain), which is responsible for product release. Recently, X. Sunney Xie and his co-workers developed a rate theory for enzymatic cycles on a two-dimensional free-energy surface.[40] They proposed that a slow enzyme conformational coordinate can facilitate the catalytic reaction along the reaction coordinate. The strained enzyme–substrate complex in a NESS can exhibit a nonequilibrium relaxation that can lower the activation energy of the reaction. Our experimental results agreed with the prediction.

■ CONCLUSION

Observing a single molecule in action is an effective way to retrieve the intrinsic single-molecule properties and allows us to explore hidden structural heterogeneity of the molecule. We investigated the catalysis-associated conformational motions of AK1 by labeling the molecule with two identical fluorophores, one near the substrate binding site and the other at the surface of the core domain. By invoking the self-quenching effect of two like fluorophores, we can probe into the large-scale conformational dynamics of AK1 with high spatial sensitivity. We investigated the influences of Mg^{2+} and ADP on AK1 and found that Mg^{2+} binding increases the structural heterogeneity of AK1, whereas ADP binding reduces the structural heterogeneity and suppresses the conformational fluctuations of the substrate-binding domain. Our HMM analysis further shows that the photon fluctuation traces are generated by transitions among three conformational states. ADP binding suppresses the direct open-to-close transitions and promotes the intermediate state-mediated catalytic pathway. The two-time correlation functions of photon fluctuation traces from AK1 reveal asymmetry in time permutation, indicating single-molecule AK1 to be in a NESS. This finding can serve as an important foundation to deepen our insight into the molecular mechanisms of cellular biochemistry.

■ ASSOCIATED CONTENT

Supporting Information

Details of single-molecule optical measurement and relevant information about the data analysis procedure. This material is available free of charge via the Internet at http://pubs.acs.org.

■ AUTHOR INFORMATION

Corresponding Author

*E-mail: jyhuang@faculty.nctu.edu.tw.

Present Address

[¶]J.Y.H.: 1001 Ta-Hsueh Road, Hsinchu, Taiwan.

Notes

The authors declare no competing financial interest.

■ ACKNOWLEDGMENTS

The authors thank financial support from the National Science Council of the Republic of China under Grant Number NSC100-2112-M-009-015-MY3.

■ REFERENCES

(1) Palmer, A. G.; Kroenke, C. D.; Loria, J. P. Nuclear magnetic resonance methods for quantifying microsecond-to-millisecond motions in biological macromolecules. *Methods Enzymol.* **2001**, *339*, 204–238.

(2) Henzler-Wildman, K.; Kern, D. Dynamic personalities of proteins. *Nature* **2007**, *450*, 964.

(3) Hanson, J. A.; Duderstadt, K.; Watkins, L. P.; Bhattacharyya, S.; Brokaw, J.; Chu, J.-W.; Yang, H. Illuminating the mechanistic roles of enzyme conformational dynamics. *Proc. Natl. Acad. Sci. U.S.A.* **2007**, *104*, 18055–18060.

(4) Chen, Y.; Hu, D.; Vorpagel, E. R.; Lu, H. P. Probing single-molecule T4 lysozyme conformational dynamics by intramolecular fluorescence energy transfer. *J. Phys. Chem. B* **2003**, *107*, 7947–7956.

(5) Bhabha, J.; Ekiert, D. C.; Gam, J.; Wilson, I. A.; Dyson, H. J.; Benkovic, S. J.; Wright, P. E. A dynamic knockout reveals that conformational fluctuations influence the chemical step of enzyme catalysis. *Science* **2011**, *332*, 234.

(6) He, Y.; Li, Y.; Mukherjee, S.; Wu, Y.; Yan, H.; Lu, H. P. Probing single-molecule enzyme active-site conformational state intermittent coherence. *J. Am. Chem. Soc.* **2011**, *133*, 14389–14395.

(7) Agarwal, P. K.; Billeter, S. R.; Rajagopalan, P. T. R.; Benkovic, S. J.; Hammes-Schiffer, S. Network of coupled promoting motions in enzyme catalysis. *Proc. Natl. Acad. Sci. U.S.A.* **2002**, *99*, 2794–2799.

(8) Olsson, U.; Wolf-Watz, M. Overlap between folding and functional energy landscapes for adenylate kinase conformational change. *Nat. Commun.* **2010**, *1*, 111.

(9) Brut, M.; Esteven, A.; Landa, G.; Renvez, G.; Rouhani, M. D.; Vaisset, M. Atomic scale determination of enzyme flexibility and active

site stability through static modes: case of dihydrofolate reductase. *J. Phys. Chem. B* **2003**, *115*, 1616−1622.
(10) Girons, I. S.; Gilles, A.-M.; Margarita, D.; Michelsonl, S.; Monnot, M.; Fermandjian, S.; Danchin, A.; Bârzu, O. Structural and catalytic characteristics of Escherichia coli adenylate kinase. *J. Biol. Chem.* **1987**, *262*, 622−629.
(11) Lu, Q.; Wang, J. Single molecule conformational dynamics of adenylate kinase: energy landscape, structural correlations, and transition state ensembles. *J. Am. Chem. Soc.* **2008**, *130*, 4772−4783.
(12) Lu, Q.; Wang, J. Kinetics and statistical distributions of single-molecule conformational dynamics. *J. Phys. Chem. B* **2009**, *113*, 1517−1521.
(13) Wang, Y.; Gan, L.; Wang, E.; Wang, J. Exploring the dynamic functional landscape of adenylate kinase modulated by substrates. *J. Chem. Theory Comput.* **2013**, *9*, 84−95.
(14) Michalet, X.; Weiss, S.; Jäger, M. Single-molecule fluorescence studies of protein folding and conformational dynamics. *Chem. Rev.* **2006**, *106*, 1785−1813.
(15) Kapanidis, A. N.; Strick, T. Biology, one molecule at a time. *Trends Biochem. Sci.* **2009**, *34*, 234−243.
(16) Hermanson, G. T. *Bioconjugate techniques*; Academic Press: New York, 2008.
(17) Gautier, I.; Tramier, M.; Durieux, C.; Coppey, J.; Pansu, R. B.; Nicolas, J.-C.; Kemnitz, K.; Coppey-Moisan, M. Homo-FRET microscopy in living cells to measure monomer-dimer transition of GFP-tagged proteins. *Biophy. J.* **2001**, *80*, 3000−3008.
(18) Doose, S.; Neuweiler, H.; Sauer, M. Fluorescence quenching by photoinduced electron transfer: a reporter for conformational dynamics of macromolecules. *ChemPhysChem* **2009**, *10*, 1389−1398.
(19) Ogawa, M.; Kosaka, N.; Choyke, P. L.; Kobayashi, H. H-type dimer formation of fluorophores: a mechanism for activatable, in vivo optical molecular imaging. *ACS Chem. Biol.* **2009**, *4*, 535−546.
(20) Pabst, M.; Köhn, A. Excited states of [3.3](4,4′)-biphenylophane: the role of charge- transfer excitations in dimers with $\pi-\pi$ interaction. *J. Phys. Chem. A* **2010**, *114*, 1639−1649.
(21) Setiawan, D.; Kazaryan, A.; Martoprawiro, M. A.; Filatov, M. A first principles study of fluorescence quenching in rhodamine B dimers: how can quenching occur in dimeric species? *Phys. Chem. Chem. Phys.* **2010**, *12*, 11238−11244.
(22) Zhou, R.; Kunzelmann, S.; Webb, M. R.; Ha, T. Detecting intramolecular conformational dynamics of single molecules in short distance range with subnanometer sensitivity. *Nano Lett.* **2011**, *11*, 5482−5488.
(23) Wahl, M.; Gregor, I.; Patting, M.; Enderlein, J. Fast calculation of fluorescence correlation data with asynchronous time-correlated single-photon counting. *Opt. Express* **2003**, *11*, 3583.
(24) Magde, D.; Webb, W. W.; Elson, E. L. Fluorescence correlation spectroscopy. III. uniform translation and laminar flow. *Biopolymers* **1978**, *17*, 361−376.
(25) Landes, C. F.; Rambhadran, A.; Taylor, J. N.; Salatan, F.; Jayaraman, V. Structural landscape of isolated agonist-binding domains from single AMPA receptors. *Nat. Chem. Biol.* **2011**, *7*, 168−173.
(26) Pirchi, M.; Ziv, G.; Riven, I.; Cohen, S. S.; Zohar, N.; Barak, Y.; Haran, G. Single-molecule fluorescence spectroscopy maps the folding landscape of a large protein. *Nat. Commun.* **2011**, *2*, 493.
(27) Bishop, C. M. *Pattern Recognition and Machine Learning*; Springer: New York, 2006.
(28) Bronson, J. E.; Fei, J.; Hofman, J. M.; Gonzalez, R. L., Jr.; Wiggins, C. H. Learning rates and states from biophysical time series: a Bayesian approach to model selection and single-molecule FRET data. *Biophy. J.* **2009**, *97*, 3196−3205.
(29) Chen, Y.; Müller, J. D.; So, P. T. C.; Gratton, E. The photon counting histogram in fluorescence fluctuation spectroscopy. *Biophy. J.* **1999**, *77*, 553−567.
(30) Tan, Y.-W.; Hanson, J. A.; Yang, H. Direct Mg^{2+} binding activates adenylate kinase from Escherichia coli. *J. Biol. Chem.* **2009**, *284*, 3306−3313.
(31) Pramanik, A.; Widengren, J. *Fluorescence correlation spectroscopy (FCS)*; Wiley-VCH Verlag GmbH & Co. KGaA: Weinheim, Germany, 2006.
(32) Sanchez-Andres, A.; Chen, Y.; Müllerller, J. D. Molecular brightness determined from a generalized form of Mandel's Q-parameter. *Biophy. J.* **2005**, *89*, 3531−3547.
(33) Marcinowski, M.; Höller, M.; Feige, M. J.; Baerend, D.; Lamb, D. C.; Buchner, J. Substrate discrimination of the chaperone BiP by autonomous and cochaperone-regulated conformational transitions. *Nat. Struct. Mol. Biol.* **2011**, *18*, 150.
(34) Wu, J. Y.; Stone, M. D.; Zhuang, X. A single-molecule assay for telomerase structurefunction analysis. *Nucleic Acids Res.* **2010**, *38*, e16.
(35) Adkar, B. V.; Jana, B.; Bagchi, B. Role of water in the enzymatic catalysis: study of ATP + AMP → 2ADP conversion by adenylate kinase. *J. Phys. Chem. A* **2011**, *115*, 3691−3697.
(36) Arora, K.; Brooks, C. L., III. Large-scale allosteric conformational transitions of adenylate kinase appear to involve a population-shift mechanism. *Proc. Natl. Acad. Sci. U.S.A.* **2007**, *104*, 18496−18501.
(37) Jana, B.; Adkar, B. V.; Biswas, R.; Bagchi, B. Dynamic coupling between the LID and NMP domain motions in the catalytic conversion of ATP and AMP to ADP by adenylate kinase. *J. Chem. Phys.* **2011**, *134*, 035101.
(38) Ruelle, D. P. Extending the definition of entropy to nonequilibrium steady states. *Proc. Natl. Acad. Sci. U.S.A.* **2003**, *100*, 3054−3058.
(39) Plotkin, S. S.; Wang, J.; Wolynes, P. G. Correlated energy landscape model for finite, random heteropolymers. *Phys. Rev. E* **1996**, *53*, 6271.
(40) Min, W.; Xie, X. S.; Bagchi, B. Role of conformational dynamics in kinetics of an enzymatic cycle in a nonequilibrium steady state. *J. Chem. Phys.* **2009**, *131*, 065104.